Chapter 6

Electron Impact on PAHs and PANHs

Electron impact ionization is one of the oldest mass spectrometric tools which focuses on identifying the possible ionization and fragmentation channels of molecules. In past, several electron impact ionization investigations have been done mainly on inert gases, diatomic or triatomic molecular gases within the range of 70 - 100 eV beam energy [154]. Several experiments and modeling attempts have been made for such studies with electron energy up to a few keV [155–157]. But such studies are very rare for larger molecules due to the complexity from numerous decay channels and difficulties in separating direct and indirect ionization processes. Target specific energy loss modeling in charged particle interaction with molecules has been attempted in some specific cases [158].

The complexity of mass spectrometric studies in polyatomic molecules arises from the fact that several indirect ionization/fragmentation channels are present in such molecules [59, 159]. Such indirect processes span a large range of decay time constants and are often nested, leading to difficulties in identification of a channel and interpretation [160]. In the context of PEPICO spectroscopy, the excess energy left in the molecule after the photo-ionization process plays a vital role in deciding the decay pathways of the molecular ions [59]. Similarly, in the case of charged particle interactions, the mechanism of energy loss decides the internal energy of the recoil ions and possible decay channels [14,161]. In the past few years, plasmon excitation in fullerene and PAHs have been shown to be a very prominent indirect ionization channel [35, 161]. For fullerene, the plasmon excitation is centered around 21 eV energy and is shown to cause the ionization of C_{60} molecule [35]. The residual energy is shared between the outgoing electron and the internal heating of the fullerene molecule. In the case of PAHs, the plasmon excitation peak is at 17 eV and it has been shown recently to cause internal heating of the molecule by an amount of 8 to 9 eV [14, 161]. It is also seen that acetylene C_2H_2 loss comes as a by-product of such plasmon excitation with a very specific range of decay constants.

Electronic delocalization plays a crucial role in deciding the stability of aromatic molecules. This delocalization gives rise to very interesting properties in molecules like polycyclic aromatic hydrocarbons (PAHs) and is the reason behind their abundant existence in the interstellar medium as well as in the earth's atmosphere [162, 163]. Therefore any radiation damages to such molecules cannot be assessed without taking into account the spread in the electron density for a given molecular orbital and, in some cases resulting in the collective behavior [27, 35, 60, 161, 164]. Photoinduced ionization and dissociation remain the most selective measurement in terms of the internal energy deposited into the molecules by the radiation. Most commonly known techniques for such measurements are the PEPICO and T-PEPICO spectroscopy [36]. In these experiments with the help of the energy analysis of emitted electrons, a precise value of the internal energy and therefore a very narrow range of decay constants can be experimentally obtained for a given statistical dissociation channel [59, 160]. On the other hand charged projectiles would deposit a broad range of energies, hence making the process of estimating the internal energy very complex, even if the secondary electron energy is tracked. Thus it becomes impractical to use conventional ToF mass spectroscopy techniques to study the dynamics of statistical decay in charged particle collisions.

A molecular system with a given internal energy is prone to decay by statistical decay process. This process is usually modeled as an Arrhenius type unimolecular dissociation process. The decay constant for such evaporation channel is given as,

$$\mathrm{k} = \mathrm{A}\mathrm{e}^{(\frac{\mathrm{E_a}}{\mathrm{k_B T}})}, \tag{6.1}$$

where A is the frequency factor, $\mathrm{E_a}$ is the barrier energy for decay, $\mathrm{k_B}$ is Boltzmann constant and T is the temperature due to the internal energy of the molecule. For a given internal energy of the molecule, the decay curve will be exponential in time. But for a range of internal energies, the decay function will be a more complex combination of multiple exponential decays due to a range of decay constants.

In this work, an attempt is made to investigate the interaction of high-energy electron beam with PAH and PANHs, then assess the time dependence of $\mathrm{C_2H_2}$ evaporation in comparison with the other channels using a TOF mass spectrometer. In electron im-

pact experiment, permanent extraction field for recoil ion is to be compensated, since it could affect the projectile beam adversely [142], which in turn can affect the range of usable beam energies. Pulsed extraction of recoil ion is an alternate method, which offers a possibility of having a variable delay between the formation and extraction of recoil ion. But the main disadvantage of this method is the relatively poor mass resolution [165] owing to which the technique is applied less often. A few systematic measurements using this technique in the electron-molecule collision have been reported recently [166], in which delayed extraction time-of-flight (DEToF) was employed in order to measure kinetic energy distributions of electron- molecules collision products and disentangle different fragmentation pathways and moieties with the same mass-to-charge ratio. We have implemented the same technique of DEToF here, to investigate the time-dependent population of the produced fragments in high-energy electron-PAH collision.

6.1 Delayed Extraction Time-of-Flight

The versatility of our electron-ion coincidence experimental set-up enables us to explore a rather uncommon technique of delayed extraction time-of-flight (DEToF) [Figure 6.1]. The pulsed extraction of ions in a ToF setup can be used to analyze the evolution of a time-dependent population of various fragmentation channels of PAHs and PANHs. If the decay constants are in the range of $10^5 - 10^6$, then it becomes possible to probe the system within sufficient time so that the thermal velocity dispersion does not affect the collection efficiency. Though such a system has limited applicability, it has helped in the present investigation to assess the evaporative loss from a PAH/PANH molecule due to electron impact. The instrumentation presented here is very effective under such conditions.

Astro-biologically important statistical dissociation channels of the PAHs and PANHs are probed using DEToF. We choose naphthalene as our PAH sample, its two derivatives quinoline, and isoquinoline as PANHs since it exhibits all the properties of large PAHs/PANHs even though it is the smallest in that class. Generally, for naphthalene and its nitrogen-containing derivatives, the loss of H and C_2H_2/HCN are the most dominant

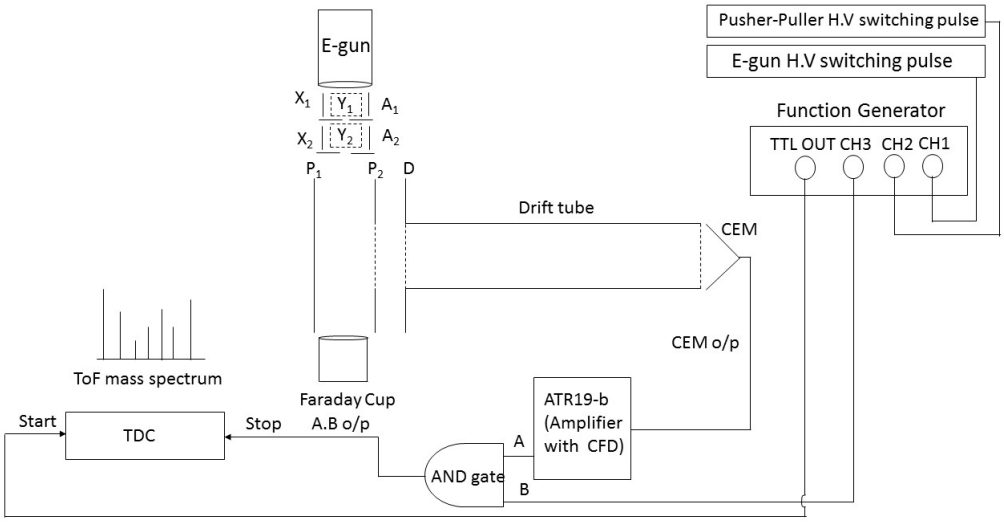

Figure 6.1: DEToF experimental schematic (first acceleration region: region between P_1 and P_2, second acceleration region: region between P_2 and D)

statistical dissociation channels. Statistical decay channels show increasing the yield of daughter ions as a function of extraction delay in the order of 10^6 s^{-1} decay constant, whereas the yields due to fast dissociation channels were observed to decrease as a function of extraction delay. On the basis of the projectile beam energy dependence of the yield, the effect of plasmon excitation in quinoline and isoquinoline is shown for the first time.

6.2 DEToF Experimental Setup Details

We use a Wiley-McLaren-type ToF mass spectrometer [167] with the pulsed extraction technique for detection of the product-ions. The schematic diagram of the experimental set-up with the data acquisition module is shown in Figure 6.1. The spectrometer consists of a pusher (P_1) as well as puller (P_2) plate of thickness 1 mm and an outer diameter of 105 mm. The puller plate has an opening diameter of 26 mm and is covered with a nickel mesh characterized by 16 lines per cm, for field uniformity. This allows a transmission efficiency of 95% of the ions. For the field-free drift of ions, we have a drift tube of length 200 mm with an opening of 25 mm covered by a nickel mesh for field uniformity, which is identical in characteristics to the one used for covering the opening of the puller plate.

The gap between the pusher (P_1) and puller plates (P_2) is 16 mm while that between the puller and the drift tube is 5 mm. A home-built, low current high energy (1-5 keV) electron gun is used for ionizing the target molecule. The filament produces electrons via thermionic emission with a heating current of about 180 mA. Two sets of XY deflectors are mounted beyond the focusing lens. We use two apertures (A_1, A_2), one between the two deflector sets (A_1) and the other after the deflectors (A_2), to avoid the secondary electrons from the internal scattering of the beam to reach the interaction region. The energy of the electron beam is decided by the floating voltage of the whole electron gun assembly. The electron gun operates in a pulsed mode with a variable ON time width. For pulsed extraction ToF, we have used home-built high voltage MOSFET switches, which can switch the high voltage in the push-pull mode with a 50 ns rise and fall time. A cylindrical shaped Faraday cup of length 100 mm and radius of 25 mm, biased to +36 Volts is used to collect the projectile electrons. The target molecule is introduced into the interaction zone that is well localized in space through a fine capillary of internal diameter 300 microns and length of 15 mm. The capillary exit is kept nearly 5 mm away from the center of the ToF interaction region to avoid any possible secondary electron emission due to the electron beam colliding with the capillary. We have used a channeltron (CEM) for the detection of ions, with a bias voltage of -2600 Volts. In addition, we pulse the electron gun and the pusher-puller plates for delayed ToF mass spectrometry as per the pulsing sequence is shown in Figure 6.2. Ions produced in the interaction region (region between P_1 and P_2) are accelerated by the electric field and compensated for the spatial spread in the second region (region between P_2 and D) before entering the field-free drift tube followed by the ion detector. The data is acquired using a multi-hit time-to-digital converter data acquisition system (Agilent TDC Model: U1051A). A gate pulse is used to filter out the switching noise picked up by the detector channel.

The target sample vapor was introduced into the setup at room temperature in which the RMS velocity of the molecules is$\sim$ 240 μm/μs. Thus, it is very important to design the ToF in such a way that the drift of target molecules between the electron pulse and the extraction pulse do not reduce the collection efficiency. It is important to account for the extraction pulse rise time in order to have a constant collection efficiency over different extraction delays. This was achieved by using high extraction field of 125 V/cm

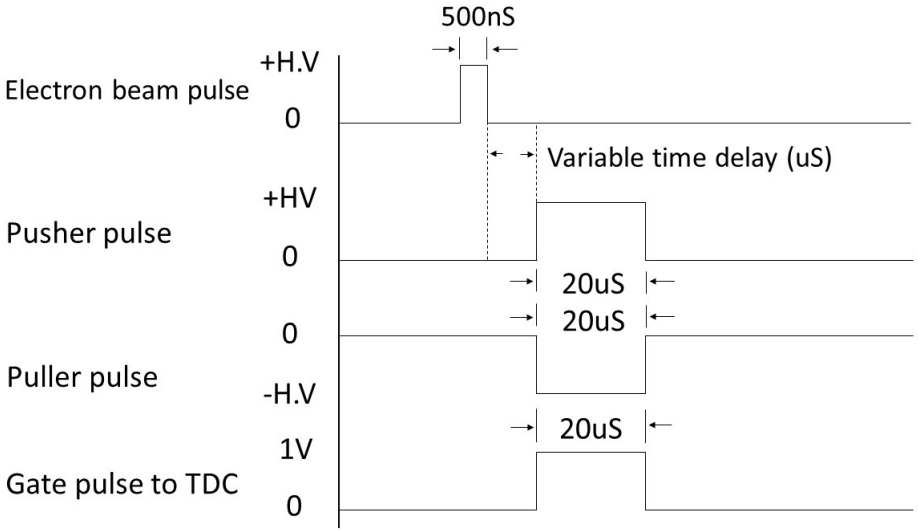

Figure 6.2: Pulsing sequence for DEToF

(interaction region). By doing an ion trajectory simulation with the help of SIMION8.0 we arrived at these settings. To check the collection efficiency, the simulations are done with all the three molecules by a spherical distribution of the source of diameter 6 mm and an RMS velocity twice as large as the value at 300 K, that is 480 μm/μs as the worst case scenario.

6.3 Analysis and Results

The typical mass spectra for the three cases are shown in Figure 6.3. The major mass peak groups can be identified with appropriate carbon and nitrogen-containing fragments. Due to the proximity of nitrogen and carbon mass in the ToF and considering the possibilities of multiple H atoms attached to a fragment, it becomes very important to distinguish the exact mass value with an error that is better than 0.5 amu at 64.5 amu and 1 amu at 129 amu, particularly for the doubly charged channels. In order to achieve this and in the absence of higher resolution mass spectral data of these molecules we used our own mass spectra measured in a separate experiment at high energy proton beam collisions with naphthalene, quinoline, and isoquinoline (not shown here). With the help of these mass spectra, we ascertain the possible decay channels in the mass spectra to be expected.

We have considered the following groups of decay channels for our analysis. The

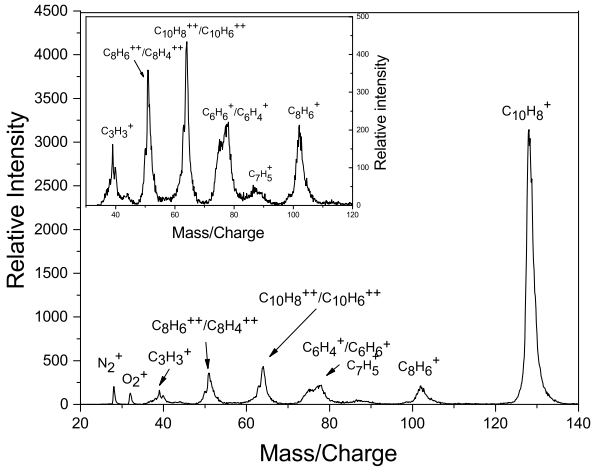

(a)

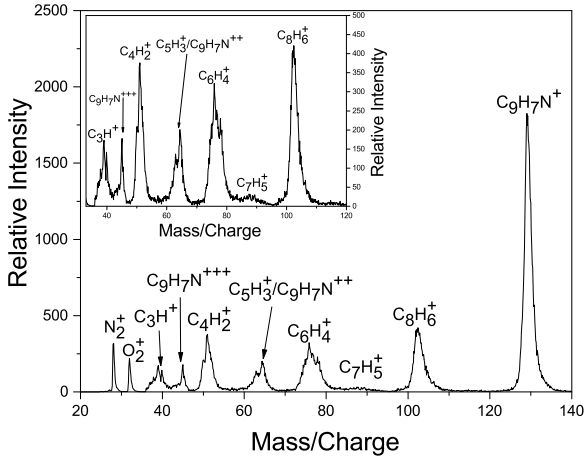

(b)

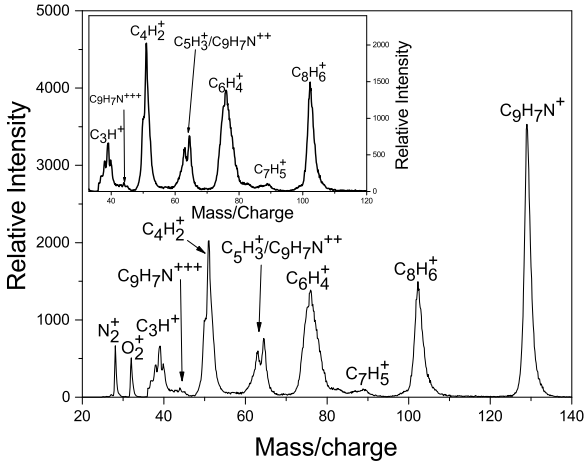

(c)

Figure 6.3: Typical Mass Spectrum of (a) Naphthalene ($C_{10}H_8$) (b) Quinoline (C_9H_7N) (c) isoquinoline (C_9H_7N) at 1000 eV electron impact (Inset:in figure (a) fragments of naphthalene, (b) fragments of quinoline, (c)fragments of isoquinoline)

yields are obtained from the mass spectra of each of the mass groups. The other possible channels are generally of negligible intensity and hence they are not expected to affect the yield ratios for a given group.

I) Naphthalene

1. $C_{10}H_8 + e^- \rightarrow C_{10}H_8^+ + 2e^-$

2. $C_{10}H_8 + e^- \rightarrow C_8H_6^+ + C_2H_2 + 2e^-$
   $C_{10}H_8 + e^- \rightarrow C_8H_5^+ + C_2H_2 + H + 2e^-$

3. $C_{10}H_8 + e^- \rightarrow C_6H_6^+ + C_4H_2 + 2e^-$
   $C_{10}H_8 + e^- \rightarrow C_6H_5^+ + C_2H_2 + C_2H + 2e^-$
   $C_{10}H_8 + e^- \rightarrow C_6H_4^+ + C_4H_4(2 \times C_2H_2) + 2e^-$

4. $C_{10}H_8 + e^- \rightarrow C_5H_3^+ + C_2H_2 + C_3H_3 + 2e^-$

5. $C_{10}H_8 + e^- \rightarrow C_4H_4^+ + C_4H_2 + C_2H_2 + 2e^-$
   $C_{10}H_8 + e^- \rightarrow C_4H_3^+ + 2 \times C_2H_2 + C_2H + 2e^-$
   $C_{10}H_8 + e^- \rightarrow C_4H_2^+ + 3 \times C_2H_2 + 2e^-$

6. $C_{10}H_8 + e^- \rightarrow C_3H_3^+ + C_3H_3 + C_4H_2 + 2e^-$

7. $C_{10}H_8 + e^- \rightarrow C_{10}H_8^{++} + 3e^-$
   $C_{10}H_8 + e^- \rightarrow C_{10}H_6^{++} + 2H/H_2 + 3e^-$

8. $C_{10}H_8 + e^- \rightarrow C_8H_6^{++} + C_2H_2 + 3e^-$
   $C_{10}H_8 + e^- \rightarrow C_8H_4^{++} + C_2H_2 + 2H/H_2 + 3e^-$

II) Quinoline and Isoquinoline

1. $C_9H_7N + e^- \rightarrow C_9H_7N^+ + 2e^-$

2. $C_9H_7N + e^- \rightarrow C_8H_6^+ + HCN + 2e^-$
   $C_9H_7N + e^- \rightarrow C_8H_5^+ + H_2CN + 2e^-$

3. $C_9H_7N + e^- \rightarrow C_7H_5N^+ + C_2H_2 + 2e^-$
   $C_9H_7N + e^- \rightarrow C_7H_5^+ + C_2H_2N^+ + 3e^-$

4. $C_9H_7N + e^- \rightarrow C_6H_3^+ + C_3H_4N + 2e^-$
   $C_9H_7N + e^- \rightarrow C_6H_2^+ + C_3H_5N + 2e^-$

5. $C_9H_7N + e^- \rightarrow C_5H_2N^+ + C_4H_4 + H + 2e^-$
   $C_9H_7N + e^- \rightarrow C_5H_2N^+ + 2 \times C_2H_2 + H + 2e^-$
   $C_9H_7N + e^- \rightarrow C_5H_2^+ + C_4H_5N + 2e^-$

6. $C_9H_7N + e^- \rightarrow C_9H_7N^{++} + 3e^-$
   $C_9H_7N + e^- \rightarrow C_9H_6N^{++} + H + 3e^-$
   $C_9H_7N + e^- \rightarrow C_9H_5N^{++} + H_2 + 3e^-$

7. $C_9H_7N + e^- \rightarrow C_6H_6^+ + C_3H_2N + 2e^-$
   $C_9H_7N + e^- \rightarrow C_6H_4^+ + C_5H_4N + 2e^-$

8. $C_9H_7N + e^- \rightarrow C_4H_2^+ + C_5H_5N + 3e^-$

9. $C_9H_7N + e^- \rightarrow C_3H_2N^+ + C_6H_5 + 3e^-$
   $C_9H_7N + e^- \rightarrow C_3H^+ + C_6H_6N + 2e^-$

10. $C_9H_7N + e^- \rightarrow C_9H_7N^{+++} + 4e^-$
    $C_9H_7N + e^- \rightarrow C_9H_6N^{+++} + H + 4e^-$
    $C_9H_7N + e^- \rightarrow C_9H_5N^{+++} + H_2 + 4e^-$

Generally, for PAHs and PANHs, the loss of H and C_2H_2/HCN are the most dominant statistical dissociation channels. The CEM detection efficiency, which strongly depends on the velocity of the ion hitting the detector, causes a lower detection efficiency as a function of increasing the mass of the fragment [168]. Hence the actual HCN loss intensity is higher than what appears in the mass spectrum. Since our main goal here is to compare relative yields of identical mass fragments with different targets, the efficiency correction is not expected to affect the analysis. Compared to PANHs, naphthalene clearly shows much higher stability with the fragmentation yields in comparison with the low stability of fragmentation yields of singly charged ions. Similarly, the second ionization yield is larger compared to adjacent fragment peaks in naphthalene highlighting the stability of naphthalene di-cation over the other two targets. The C_2H_2 loss channel is important in naphthalene whereas HCN loss is an important channel in the other two PANHs. The activation barrier for the C_2H_2/HCN loss has been reported for naphthalene, quinoline and isoquinoline to be 4.13 eV [160], 4.17$\pm$0.05 eV and 4.03$\pm$0.05 eV [12] respectively. The kinetic shift, i.e. the excess energy required to have the decay constant in the order of $10^6 s^{-1}$ for C_2H_2 loss in naphthalene is about 4.2 eV whereas for the HCN loss in the PANHs considered here it is about 2.7 to 3 eV, which is calculated using the Rice-Ramsperger-Kassel-Marcus quasi-equilibrium theory (RRKM/QET) [160]. Thus, it is expected that the PANHs show a much larger yield of HCN loss compared to the C_2H_2 loss in naphthalene. For the *decay channel no. 5*, in this time scale, the mechanism of formation is less clear and hence it is hard to associate it with any individual decay process. The other fragments are much stronger in PANHs. The most significant observation is a higher tendency of isoquinoline compared to quinoline towards fragmentation. Both PANHs show a H_3 loss in the double ionization peak as the prominent channel. The origin

of this channel is difficult to ascertain. A similar peak is seen in naphthalene but with the H_2 loss. The intensity of H_2 or H_3 loss at the double ionization peak is quite significant. $C_6H_4{}^+$ region shows a clear difference in the peak shape across the three examples. This indicates a difference in the decay channel which again could be related to the location of the nitrogen atom in the ring.

6.3.1 Normalisation and Beam Energy Dependence

HCN loss shows the strongest intensity compared to adjacent mass peaks in quinoline and isoquinoline hence other channels in this mass group are neglected in the rest of the analysis. The yields in each spectrum are normalized with the total area of the single ionization peak, including neutral H loss. The total counts in each area were much larger than 10000. Thus, the systematic errors are canceled due to self-normalization with the single ionization peak and the statistical error was much smaller than the symbol size used in all the subsequently shown figures. First, we compare the relative yields as a function of the impact energy in all the three targets. This trend is shown in Figure 6.4a, 6.4b and 6.4c. Here we notice the first indication that C_2H_2/HCN loss is different from the other channels. It is very clear that C_2H_2 and HCN channel in naphthalene and (iso)quinoline, respectively show a much slower change in the yield as compared to all the other channels. The other channels show almost an identical variation of rapid decrease within a given target species. This effect has also been observed with ion impact on naphthalene and is attributed to plasmon excitation process [34]. We observed similar features in the nitrogen derivatives as well. This shows that the presence of one nitrogen atom does not affect the collective excitation process.

The mass spectra are recorded and the relative yields in the target and incident beam energy combinations are plotted as a function of the extraction delay for each individual channel. Figure 6.6 shows the data for naphthalene at a beam energy of 250 eV. The relative yields clearly show two types of decay channels. One set shows a systematic decrease in magnitude as we increase the delay and the other shows either a constant or small increase in intensity that stabilizes within 5 microsecond time scale. A similar behavior is seen in all the other beam energies. In the case of naphthalene, these slow changing or

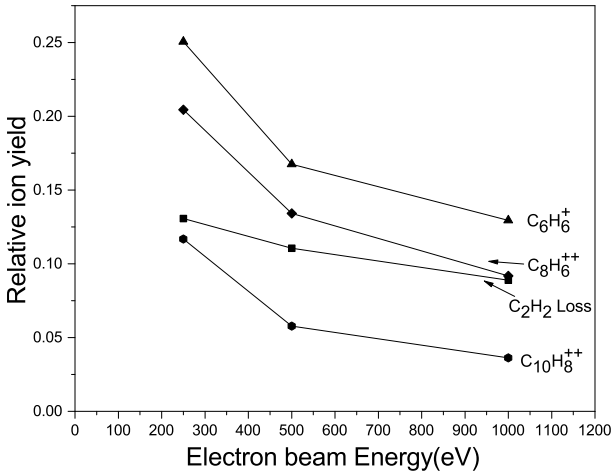

(a)

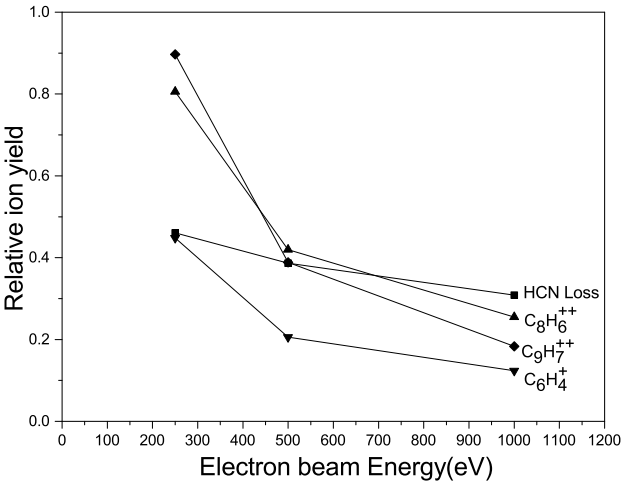

(b)

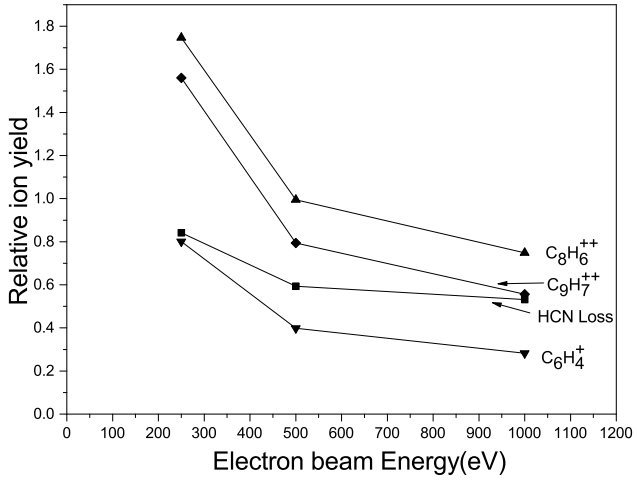

(c)

Figure 6.4: Energy dependence of different decay channels with zero delay time extraction (a) Naphthalene (b) Quinoline (c) Isoquinoline molecules

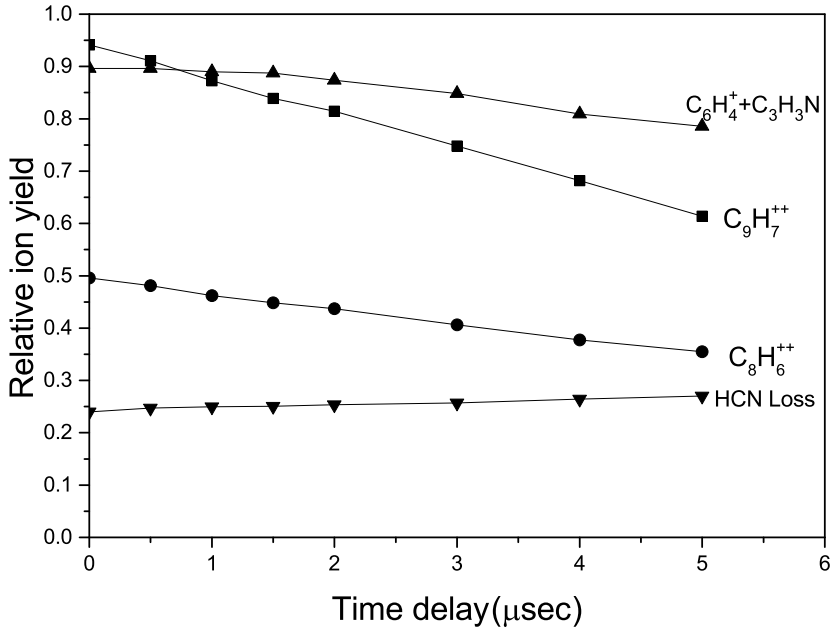

(a)

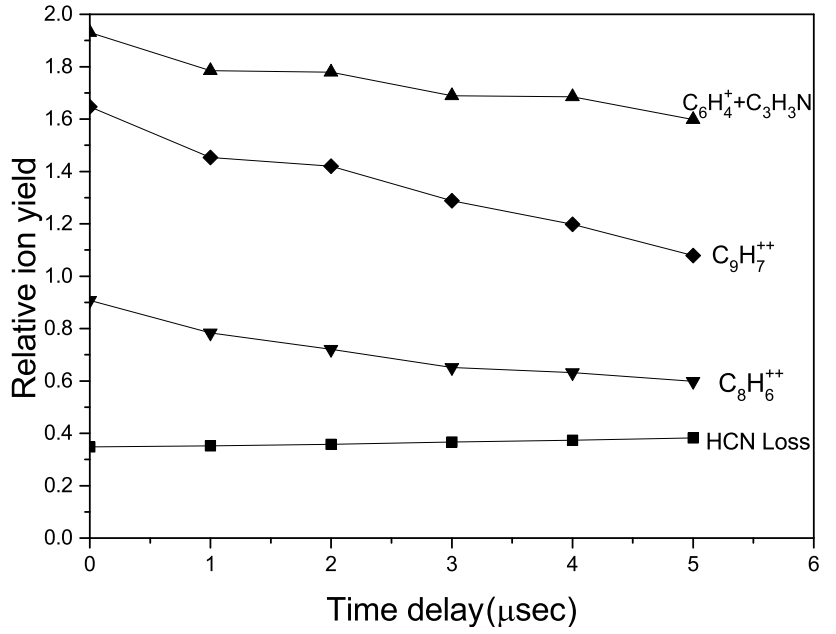

(b)

Figure 6.5: Various dissociative and violent decay channels with delay time extraction (a) Quinoline (b) Isoquinoline molecules under 250 eV electron impact

increasing channels are clearly related to the statistical dissociation channels [87, 160]. Figure 6.5a and 6.5b, show the similar measurements for quinoline and isoquinoline at 250 eV. Here, the behavior is again similar to naphthalene except that the relative yields for corresponding channels are higher and the time evolution of the two slow channels is different. The statistical channels for naphthalene have been reported in the literature

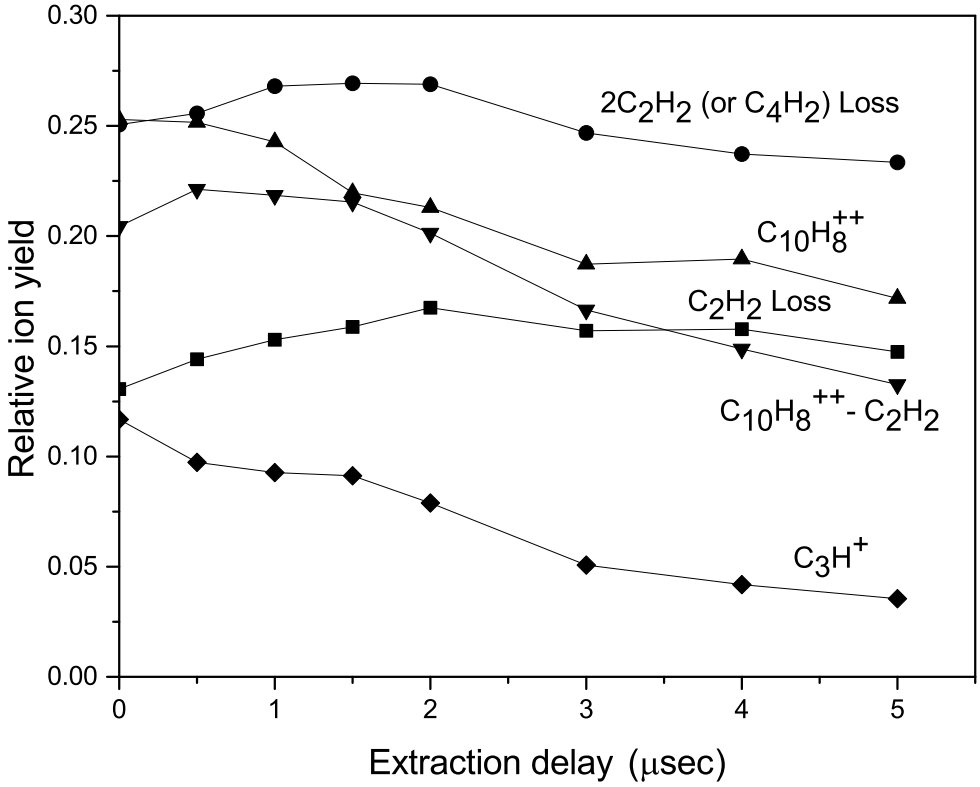

Figure 6.6: Various violent and dissociative decay channels with delayed extraction time for naphthalene under 250 eV electron impact

but for quinoline and isoquinoline, such detailed studies are not available. Bouwman *et al*. (2015) have discussed H loss and HCN loss in one of the recent photodissociation studies for the two cases but the second slow channel seen here is not discussed in the literature [104]. Using the list of decay channels and their mechanisms it is easy to identify that the HCN loss and C_3H_nN are the dissociation channels with microsecond timescale whereas all other channels decay at a much faster rate with sufficiently large kinetic energy release (KER) to diffuse from the interaction region rapidly. In particular, the doubly charged species (decay channel) is likely to further dissociate to smaller singly charged fragments. Consequently, the population of the intact dication and dication-HCN also decrease rapidly as seen in the data. We compare our results with the NIST data taken at 70 eV [107]. The mass spectra show the same decay channels as our case but with a strong variation in the yields. For both PANHs the mass spectra are almost identical yields for respective decay channels at 70 eV. In contrast, we observe clearly that isoquinoline is more prone to decay by fragmentation than quinoline.

6.3.2 HCN Loss Channel in Quinoline and Isoquinoline

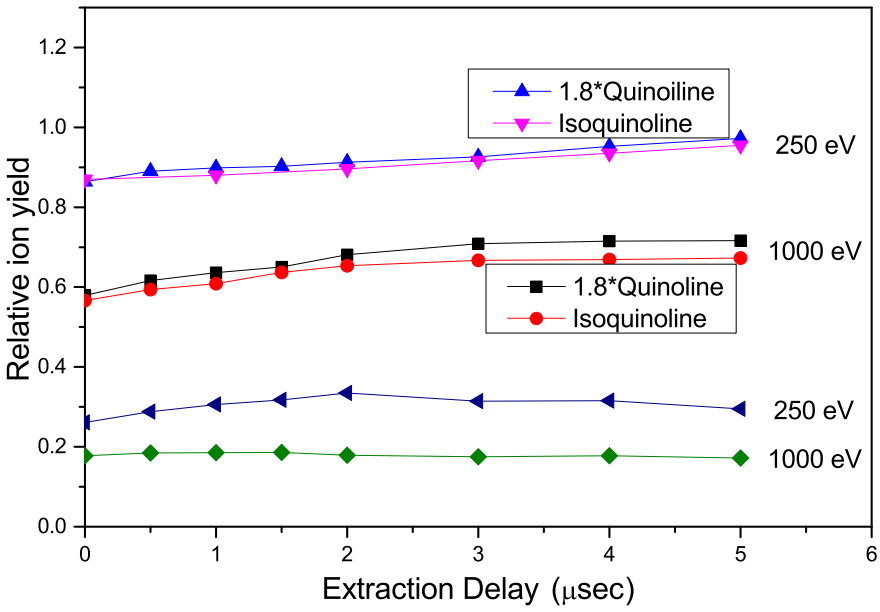

Figure 6.7: HCN/C_2H_2 loss channel in naphthalene, quinoline and isoquinoline

The HCN elimination process in both the PANHs studied here is known to depend on the pairing of the nitrogen atom with the nearest carbon atom. In the case of quinoline at 70 eV electron impact, 33% yield of HCN was seen to arise from one of the adjacent carbon atoms [12]. The other atom in one of the shared carbon between two rings was not found to contribute significantly. On the other hand, for isoquinoline, the nitrogen position was found to help in pairing with either of the two carbons, contributing to nearly 70% of the HCN yield [13]. Moreover, at low energy neutral impact, the process was entirely governed by pairing with the adjacent carbon atoms and the carbon randomization was found to be absent [12, 13]. This work directly demonstrates that the relative yield of HCN loss for quinoline is approximately half (0.555) of that from isoquinoline. On the other hand, we found that the decay constants for HCN loss are of the order of $10^6 s^{-1}$ and are almost identical in both PANHs.

At all the three beam energies, the HCN loss channel in quinoline and isoquinoline show a strong similarity in the evolution of the relative yield which follows exactly the same time scale as shown in Figure 6.7. This highlights very clearly that the mechanism of formation of HCN in the two cases must be identical. A detailed discussion regarding the elimination of HCN from these two species can be found in the very recent work

by Bouwman et al [104]. The observations here are consistent with their experimental results on photodissociation. Having noted this, the two examples drastically differ in the magnitude of the relative yields. As shown in Figure 6.7 the HCN loss yield in quinoline is multiplied by a factor of 1.8 to match with that of the isoquinoline, which clearly shows that the possibility of losing HCN from quinoline is approximately half of that of from isoquinoline as shown by the structure calculations in Section 2.1 in the Chapter 2. This factor remains the same for all the beam energies. Such a comparison of yields under identical conditions is not reported so far to the best of our knowledge.

6.3.3 HCN+C_2H_2 Loss Channel in Quinoline and Isoquinoline

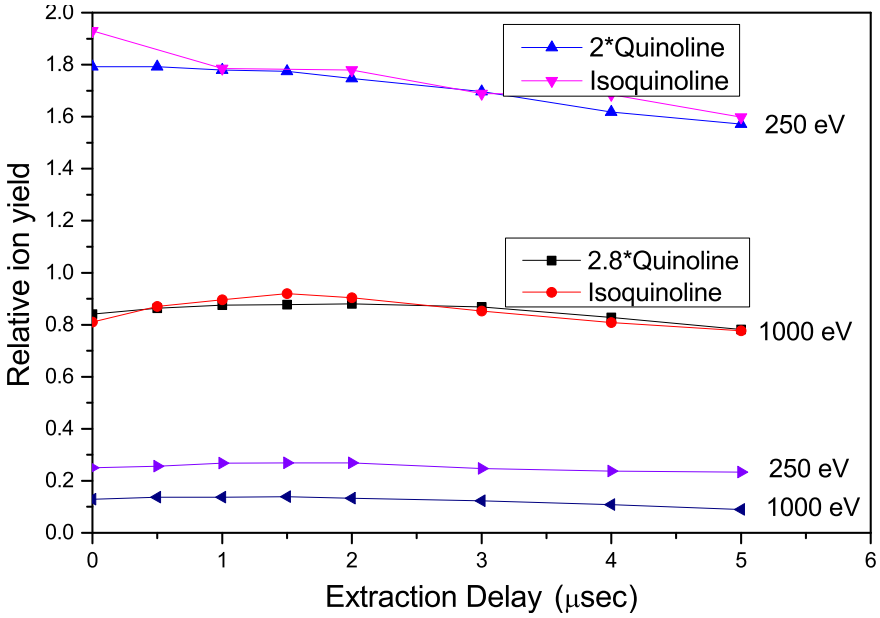

Figure 6.8: HCN+C_2H_2 loss channel in quinoline and isoquinoline

In the case of naphthalene, the loss of diacetylene and 2 times the loss of C_2H_2 are competing channels with the diacetylene loss being the significantly larger channels as seen in figure 6.3. Structurally, both the rings in naphthalene can produce diacetylene fragment. In quinoline and isoquinoline, on the other hand, 76 amu has a higher intensity than 78 amu. The minimal intensity of 79 amu indicates diacetylene loss is negligible. This leaves the ring with nitrogen to produce the neutral fragment with the corresponding ion at 76 and 78 amu. There are two possibilities in this mass region, first is the loss of HCN + C_2H_2, giving rise to the fragment of mass 76. The other possibility is the loss

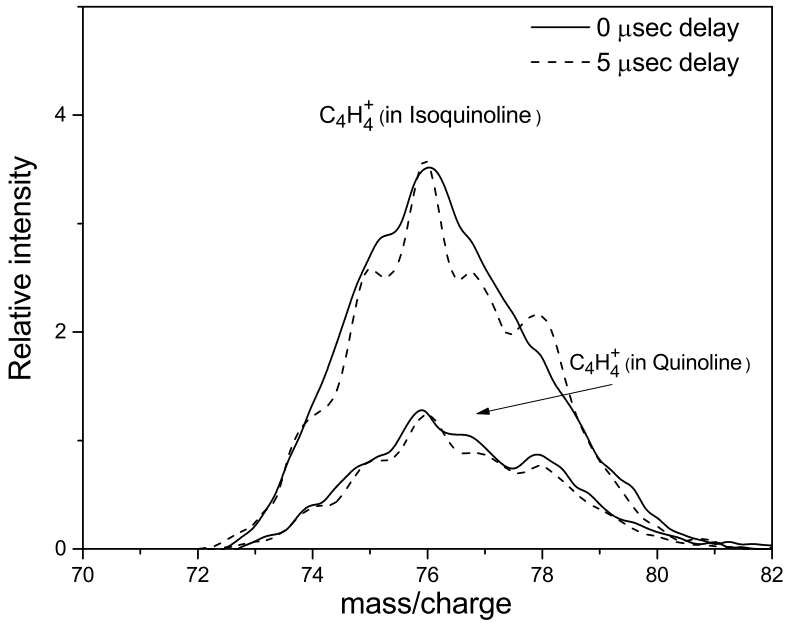

Figure 6.9: HCN+C_2H_2 loss channel overlapped mass spectrum in quinoline and isoquinoline

of propiolonitrile (C_3NH) resulting in a fragment of mass 78. Due to the lack of previous investigations towards this aspect, it has not been possible to quantify and compare these two channels energetically. As we can see in Figure 6.3, quinoline shows a higher intensity of 76 mass compared to rest of the fragments in the vicinity. This is in contrast to isoquinoline spectrum. Considering the structure of propiolonitrile (C_3NH), it is expected that quinoline should have a higher probability of HCN + C_2H_2 loss compared to isoquinoline. In terms of time evolution, this channel shows an initial increase up to 1.5 microseconds and thereafter a rapid decrease for isoquinoline at 1000 eV beam energy. For quinoline, this change is much slower and it peaks at about 3 microseconds. The yield variation is as much as 20% from the zero delay to the peak yield for isoquinoline and about 12% for quinoline at 1000 eV. At 250 eV on the other hand, the decrease is very rapid in both the targets as can be seen in Figure 6.8.

To this end, it is observed that the shape of the peak in this channel also evolves with the extraction time for isoquinoline. Figure 6.9 shows the mass overlapped mass spectra for quinoline and isoquinoline in the mass range of the fragment in the discussion. It is evident that the isoquinoline structure develops sharper peaks due to the fast diffusion of higher energy fragments from the interaction region thus improving the resolution of the

mass spectrum. This behavior is very weak in quinoline. Similar to HCN loss channel, this channel also shows a variation in the magnitude of the yield between quinoline and isoquinoline. The factor to be multiplied with quinoline yield to match with the isoquinoline magnitude is about 2 at 250 eV and 2.8 at 1000 eV.

The statistical decay channels of naphthalene, quinoline, and isoquinoline were observed to show a slow microsecond range decay time constant. A similar trend was seen with C_4H_2 and C_2H_2+HCN loss channel in naphthalene and (iso)quinoline, respectively. The rest of the channels show a gradual decrease in intensity as a function of delay due to rapid dispersion following a violent fragmentation. Thus the DEToF technique is used to separate the fast and slow decay channels after electron impact. A detailed analysis of HCN loss showed identical time scales in quinoline and isoquinoline but nearly twice the yield in favor of isoquinoline. We correlate this with the position of the nitrogen and the corresponding bond properties using a simplistic interpretation. A Hartree-Fock level structure calculation with GAUSSIAN09 with 3-21G basis set is used to asses the bond length variations of the targets. The observed yield variation is explained on the basis of the results. A similar analysis of diacetylene/ propiolonitrile channels shows the statistical nature of this dissociation dominating at higher electron impact energy.